

VECTORIAL ELECTRIC FIELD MONTE CARO SIMULATIONS FOR FOCUSED LASER BEAMS (800 nm–2220 nm) IN A BIOLOGICAL SAMPLE

Fuhong Cai¹, Jiaxin Yu¹, and Sailing He^{1, 2, *}

¹Centre for Optical and Electromagnetic Research, Zhejiang Provincial Key Laboratory for Sensing Technologies, JORCEP [Joint Research Center of Photonics of the Royal Institute of Technology, Lund University and Zhejiang University], Zijingang Campus, Zhejiang University (ZJU), Hangzhou 310058, P. R. China

²Department of Electromagnetic Engineering, Royal Institute of Technology, Stockholm 100 44, Sweden

Abstract—Here we develop a method that combines vectorial electric field Monte Carlo simulation with Huygens-Fresnel principle theory to determine the intensity distribution of a focused laser beam in a biological sample. The proper wavelengths for deep tissue imaging can be determined by utilizing our method. Furthermore, effects of anisotropic factor, scattering and absorption coefficients on the focal spots are analyzed. Finally, the focal beams formed by objective lenses with different values of numerical aperture are also simulated to study the focal intensity in the biological sample.

1. INTRODUCTION

Development of non-invasive imaging has gained traction over the years due to its important role in basic research and clinical diagnosis [1–3]. Optical imaging methods using near infrared light are considered harmless. However, because of the absorption and scattering of the biological sample, the optical imaging of deep tissue is still a challenge. In order to minimize the optical absorption effect, a 700 nm–900 nm optical source is usually utilized in bio-imaging [4]. The range of 700 nm–900 nm is named the transparent window for biological imaging. However, several research groups reported that 1280 nm and

Received 7 August 2013, Accepted 26 September 2013, Scheduled 9 October 2013

* Corresponding author: Sailing He (sailing@jorcep.org).

1675 nm pulse lasers are better choices in microscopy for deep tissue imaging [5–7]. Their works also raise a new question: are there other wavelengths suitable for deep tissue microscopy? In this paper we use vectorial Electric field Monte Carlo to answer this question.

Monte Carlo (MC) simulation is an excellent tool to trace the propagation of light in a biological sample [8]. In our previous study, MC simulations were used to find a better wavelength for functional near infrared spectroscopy (fNIRS) [9]. It is worth mentioning that the traditional MC method can only be used to derive the distribution of incoherent optical intensity in the biological sample. For deep tissue microscopy, laser scanning microscopy (LSM), such as confocal microscope and multi-photon microscope, is the most common setup to get micro-imaging of the biological sample [10]. The analysis of the diffraction focal spots in LSM is crucial in estimating the imaging results. However, the traditional MC cannot be utilized to study the diffraction focal spots. In our study, in order to take the vectorial diffraction into account, vectorial electric field Monte Carlo (EMC) [11–15] is utilized to simulate the focal spots in the biological sample. This way we can numerically study the coherent optical intensity of focal spots.

2. METHOD

2.1. Vectorial Electric Field Monte Carlo (EMC) Simulations

Compared with traditional MC simulation, EMC simulation is an improved method, which can simulate the multiple scattering and absorption of the electric field in a biological sample. As the wave enters the sample, it propagates along the initiate direction of the wave vector \mathbf{k} for a path length determined by the scattering coefficient. The propagation direction is changed according to Mie theory when the wave covers the current path length. Then a new path length is generated and the above process is repeated in EMC until the wave leaves from the sample or is absorbed totally by some element, e.g., water. The details of EMC simulation in biological samples can also be found in Refs. [11, 12]. In order to take the diffraction into account and simulate the focal spots, according to the Huygens principle, the simulated wave is decomposed into a set of secondary spherical sub-waves. As shown in Fig. 1, an aplanatic lens system (a well-designed objective, NA = 0.6) is utilized to focus the input laser beam into the biological sample. The input beam can be considered as a plane wave of right circular polarization. According to the vectorial diffraction theory, the polarization unit vector behind the aplanatic lens will

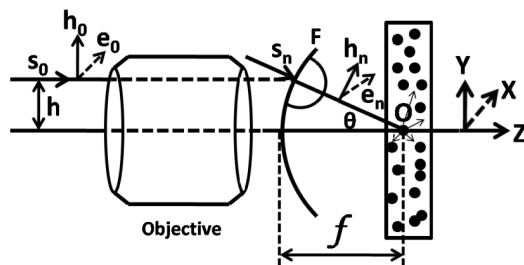


Figure 1. The diagram for the incident electrical field in the EMC simulation. The secondary spherical sub-waves are launched from the focused spherical wave-front F and then enter the biological sample. After that step, the wave is multiply scattered and absorbed by the biological sample according to the EMC process.

become $[P_x, P_y, P_z]^T \times V(\psi, \varphi)$, where

$$V(\psi, \varphi) = \begin{bmatrix} 1 + (\cos \psi - 1) \cos^2 \varphi & (\cos \psi - 1) \cos \varphi \sin \varphi & -\sin \psi \cos \varphi \\ (\cos \psi - 1) \cos \varphi \sin \varphi & 1 + (\cos \psi - 1) \sin^2 \varphi & -\sin \psi \sin \varphi \\ \sin \psi \cos \varphi & \sin \psi \sin \varphi & \cos \psi \end{bmatrix} \quad (1)$$

and where ψ and φ are the deflection angle and azimuthal angle of the propagation direction of the secondary spherical sub-wave in the image plane. $[P_x, P_y, P_z]$ is the previous polarization unit vector (for the incident wave). The secondary spherical sub-wave will enter the biological sample. The complex electric field is described by coordinate system $(\mathbf{m}, \mathbf{n}, \mathbf{s})$, where \mathbf{m} and \mathbf{n} are the unit vectors of the parallel and perpendicular components of the complex electric field vector (i.e., $\mathbf{E}_0 = e_1 \mathbf{m} + e_2 \mathbf{n}$), and \mathbf{s} characterizes the propagation direction. As the wave covers the first free path l with respect to the scattering coefficient of the medium, it undergoes Mie scattering. After one scattering, the coordinate system is updated by:

$$\begin{pmatrix} \mathbf{m}' \\ \mathbf{n}' \\ \mathbf{s}' \end{pmatrix} = \begin{pmatrix} \cos \theta \cos \phi & \cos \theta \sin \phi & -\sin \theta \\ -\sin \phi & \cos \phi & 0 \\ \sin \theta \cos \phi & \sin \theta \sin \phi & \cos \theta \end{pmatrix} \begin{pmatrix} \mathbf{m} \\ \mathbf{n} \\ \mathbf{s} \end{pmatrix} \quad (2)$$

and the complex electrical field is updated by:

$$\begin{pmatrix} e'_1 \\ e'_2 \end{pmatrix} = [F(\theta, \phi)]^{-1/2} \begin{pmatrix} S_2 \cos \phi & S_2 \sin \phi \\ -S_1 \sin \phi & S_1 \cos \phi \end{pmatrix} \begin{pmatrix} e_1 \\ e_2 \end{pmatrix} \quad (3)$$

where $F(\theta, \phi)$ is the light intensity normalization factor [14]:

$$\begin{aligned}
 F(\theta, \phi) = & \left(|S_2|^2 \cos^2 \phi + |S_1|^2 \sin^2 \phi \right) |e_1|^2 \\
 & + \left(|S_2|^2 \sin^2 \phi + |S_1|^2 \cos^2 \phi \right) |e_2|^2 \\
 & + 2 \left(|S_2|^2 - |S_1|^2 \right) \cos \phi \sin \phi \operatorname{Re} [e_1(e_2)^*] \quad (4)
 \end{aligned}$$

and where θ and ϕ are scattering and azimuthal angles, respectively; S_1 and S_2 are the complex scattering amplitudes [11]. The electric field would become $E_1 = [e'_1 \mathbf{m}' + e'_2 \mathbf{n}'] \exp(ikl)$ after one scattering and the photon weight w is updated by $\exp(-\mu_a l)w$, where μ_a is the absorption coefficient of the biological sample. The above process is repeated in EMC simulation until the wave leaves from the sample or the value of photon weight w becomes too small [8]. In this paper, parts of the simulation results agree well with some published experimental data (see Section 3), which can also be used to verify our new method.

2.2. The Optical Parameters in the EMC Simulations

The biological sample simulated in this paper is assumed to be an aqueous phantom containing 1- μm -diameter scattering beads at a concentration of 0.1044 spheres/micron³. The main absorption element in the sample is water, whose absorption spectrum is shown in Fig. 2(a) [16]. The scattering coefficient is calculated by Mie theory, in which the refractive index of the background medium (i.e., water) is derived from Ref. [17] and the refractive index of the scattering beads is obtained according to the Cauchy dispersion equation [18]:

$$n_r = A + B/\lambda^2 + C/\lambda^4 \quad (A = 1.3696; B = 3916.8; C = 2558.8) \quad (5)$$

The scattering coefficients are shown in Fig. 2(b). In practice, titanium sapphire pulse laser (680 nm–1000 nm) [19], Yb-doped large-mode-area photonic crystal fiber laser (1040 nm) [20], optical parametric oscillator pulse laser (1100 nm–1850 nm) [7] and soliton self-frequency shift pulse laser (about 1675 nm) [6] are available for use in non-linear imaging setup. To make our simulations more practical, the simulated wavelengths are selected as 800 nm, 1040 nm, 1280 nm, 1440 nm, 1560 nm, 1680 nm, and 1800 nm to demonstrate the performance of the aforementioned lasers in tissue imaging. To our knowledge, a longer wavelength range (> 1850 nm) is rarely studied. In our study, the focal spots of 1920 nm and 2220 nm lasers are also simulated. Through the simulations, we found that 2220 nm can also be a suitable wavelength for deep tissue imaging. The absorption and scattering coefficients of these wavelengths are marked in Fig. 2.

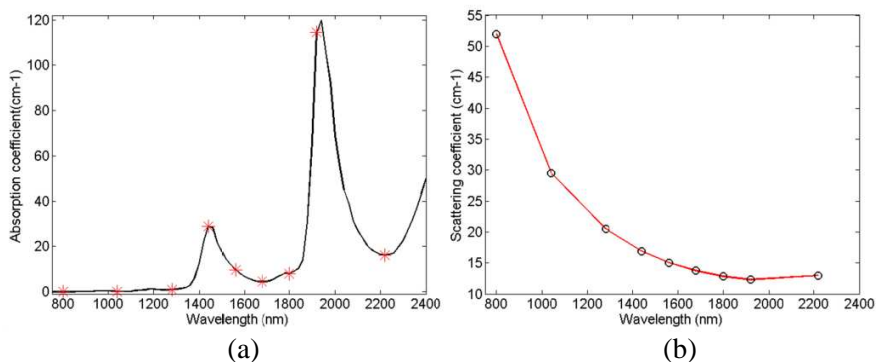


Figure 2. (a) The absorption and (b) scattering coefficients of the biological sample utilized in this study, the selections of the simulated wavelengths are discussed in Subsection 2.2.

3. RESULTS AND DISCUSSION

3.1. The Intensity Distribution of Focal Spots in Biological Sample

The results of the simulations described in Section 2 are shown in Fig. 3 and Fig. 4, which describe the intensity distribution of focal spots at depth of 0.5 mm and 1.5 mm respectively. When 9 laser lights with different wavelengths are focused into the biological sample, their focal spots are all well formed at a depth of 0.5 mm. As the wavelength increases, the size of the focal spot increases due to the diffraction. When the imaging resolution is taken into account, the 800 nm pulse laser is a most suitable optical source in multi-photon LSM. However, the scattering coefficient for the 800 nm laser (about 52 cm^{-1} in this paper) is relatively large compared with that for a long wavelength laser. As the focal depth gets larger, the number of scattering events for the propagation of the 800 nm light increases rapidly. This would deteriorate the focal intensity in the turbid medium [12]. As shown in Fig. 4, when focusing at a depth of 1.5 mm, the focal spot of the 800 nm laser almost drowned in the background noise, indicating that 800 nm is not a good choice at the depth of 1.5 mm. In 2009, Kobat et al. demonstrated that 1280 nm is a better wavelength for deep tissue micro-imaging compared with 775 nm [5]. They further illustrated that 1675 nm is also an excellent wavelength in three-photon microscopy [6]. As shown in Fig. 4, the intensities for the focal spot of 1280 nm and 1680 nm are much greater than that of 800 nm, indicating that our simulated results agree well with the published experimental

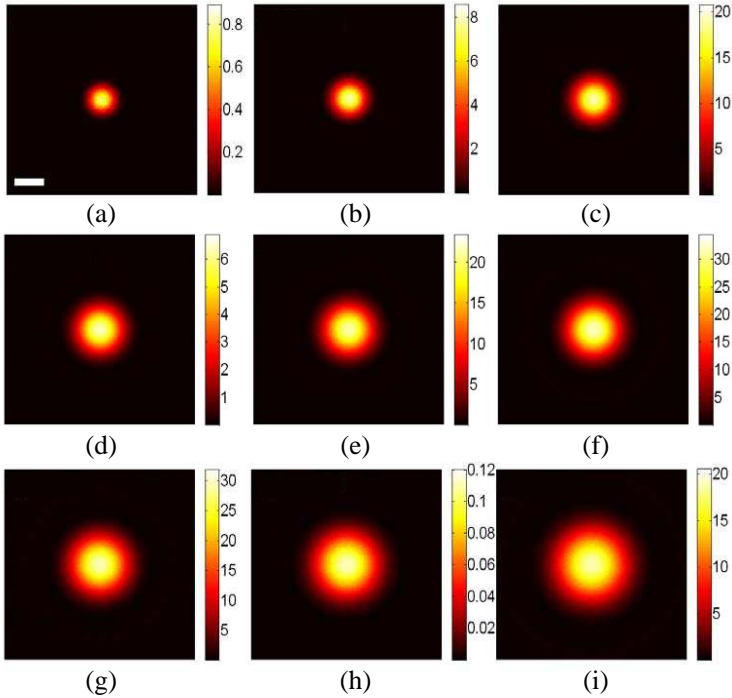


Figure 3. The EMC simulation results for the focal spots of 9 lasers with different wavelengths in the biological sample at a depth of 0.5 mm. (a) 800 nm. (b) 1040 nm. (c) 1280 nm. (d) 1440 nm. (e) 1560 nm. (f) 1680 nm. (g) 1800 nm. (h) 1920 nm. (i) 2220 nm.

results. Wang et al. also used 1600 nm–1850 nm pulse lasers to improve the depth limit of vibrational photoacoustic (VPA) microscopy [7], in which the VPA spectra of 2vCH₂ and 2vCH₃ have two peaks at around 1730 nm and 1760 nm. Therefore, considering the penetration feature of light and the VPA generation efficiency, the best wavelength is between 1700 nm and 1750 nm in Ref. [7]. From the above simulation and experimental results, we can conclude that the decrease of the scattering coefficient is good for deeper tissue imaging. However, as the wavelength gets longer, the absorption characteristic of the biological sample becomes prominent. For example, the scattering coefficient for the 1920 nm laser is relatively small (about 12.31 cm⁻¹), which is even smaller than that of 1800 nm (about 12.81 cm⁻¹), but its focal intensity drops to ‘0’ at the depth of 1.5 mm due to the extreme strong absorption coefficient of water at 1920 nm (see Fig. 2). Hence, selecting

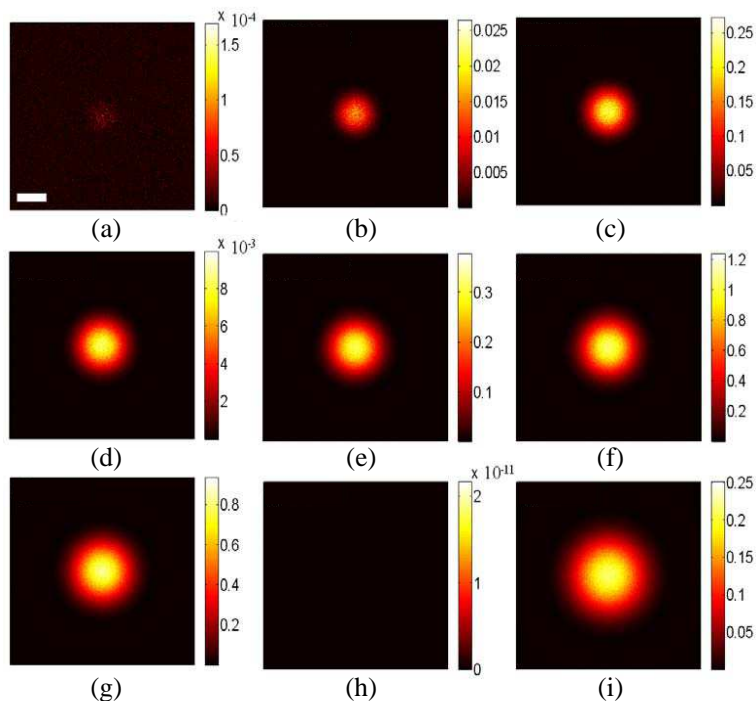


Figure 4. The EMC simulation results for the focal spots of 9 lasers with different wavelength in the biological sample at a depth of 1.5 mm. (a) 800 nm. (b) 1040 nm. (c) 1280 nm. (d) 1440 nm. (e) 1560 nm. (f) 1680 nm. (g) 1800 nm. (h) 1920 nm. (i) 2220 nm.

a NIR wavelength with a relatively small absorption coefficient is the criterion for deep tissue imaging. In the absorption spectrum of water between 1900 nm and 2400 nm, the minimum point is at 2220 nm (16.13 cm^{-1}). A simulation result of the focal spot for the 2220 nm laser at a depth of 1.5 mm is shown in Fig. 4(i), in which an excellent focal spot with a relatively strong intensity illustrates that the 2220 nm laser is also suitable for deep tissue imaging.

The focal intensity curves are shown in detail in Fig. 5. The peak intensities of the curves can demonstrate the penetration characteristics of the 9 kinds of lasers. The deviation of the three curves in each sub-figure can indicate the attenuation of the coherent intensity as the focal depth gets larger. The full width at half maximum (FWHM) of the curves can help readers to analyze the resolution within the biological sample for different wavelengths.

From the standpoint of deep tissue imaging, according to the

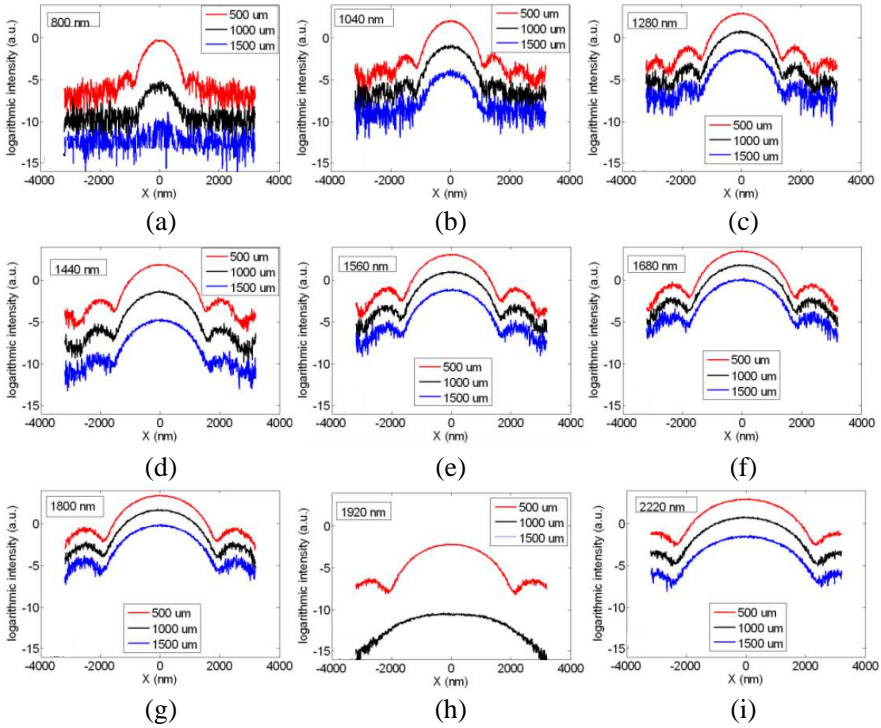


Figure 5. The intensity curves for the focal spots at depths of 0.5 mm (red curves), 1.0 mm (black curves) and 1.5 mm (blue curves). At a depth of 1.5 mm, the 1920 nm laser is almost completely absorbed by the sample; thus the focal spot of 1920 nm laser cannot be formed at a deep position such as 1.5 mm depth. The random noise in the focal spots is due to the nature of EMC simulation (which is a statistical simulation method) and the laser speckle in the biological sample. To compare the penetration of different wavelengths more clearly, the peak intensity of the focal spot as a function of wavelength is shown in Fig. 6.

peak intensity and the deviation of the three curves, 1680 nm and 1800 nm are two of the most suitable wavelengths for deep tissue micro-imaging. In order to further compare the penetration characteristic of 1680 nm and 1800 nm lasers in the biological sample, we also simulated the focal spot of these two wavelengths at 2 mm, 2.5 mm and 3.5 mm depths. The simulation results are shown in Fig. 7. At these 4 focal depths, the focal intensities of the 1680 nm optical source are all stronger than those of the 1800 nm optical source. Therefore, for the simulated medium discussed in our study, 1680 nm laser is the best

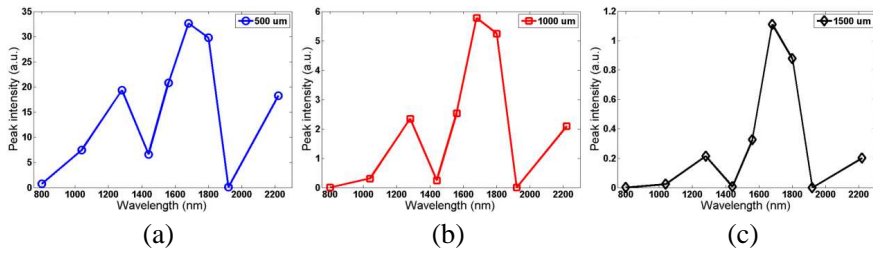


Figure 6. The intensity as a function of wavelength at different depths: (a) 500 μm, (b) 1000 μm, and (c) 1500 μm.

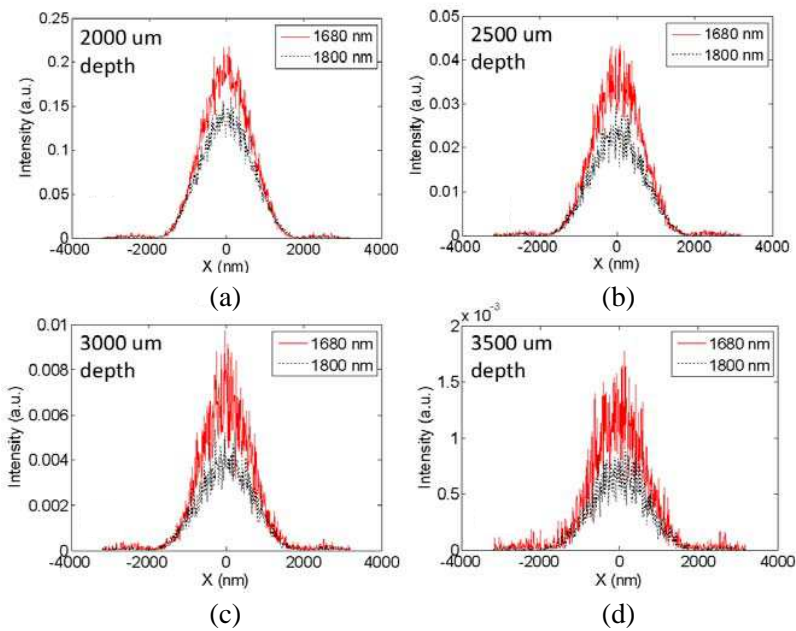


Figure 7. The focal optical intensity curves for 1680 nm and 1800 nm lasers at depth of (a) 2.0 mm, (b) 2.5 mm, (c) 3.0 mm, and (d) 3.5 mm.

choice for the deep microscopic bio-imaging.

For 1680 nm, however, as the focal depth increases from 2.0 mm to 3.5 mm, the optical intensity is attenuated by two orders of magnitude. The imaging depth limit for the existing 1680 nm pulse laser is about 1–2 mm [6]. Therefore, if we want to get the microscopic optical information of the biological sample at 3.5 mm, the optical power of the 1680 nm laser has to be increased by at least 100 times. Even

if this kind of high power optical source can be achieved, the photo-thermal damage threshold needs to be taken into account. Therefore, it is improper to extend the imaging depth limit by only increasing the laser power.

3.2. The Effect of Anisotropic Factor, Scattering and Absorption Coefficients on the Intensity of the Focal Laser Spot in Biological Sample

In tissue optics, from the standpoint of diffusive light intensity, the penetration depth of light in a biological sample is defined as:

$$1/(\mu_s(\lambda) + \mu_a(\lambda)) \quad (6)$$

where $\mu_s(\lambda)$ and $\mu_a(\lambda)$ are scattering and absorption coefficients, respectively. However, in LSM setup, the coherence has to be taken into account [12]. Four EMC simulations are performed to demonstrate the effect of anisotropic factor (g factor), as well as absorption and scattering coefficients upon the focal spot, which is at a depth of 1.5 mm. Simulation T1 is defined as a reference. In T1, the simulated wavelength is 1680 nm, and the absorption coefficient, scattering coefficient and g factor are set as 10 cm^{-1} , 10 cm^{-1} (same value as the absorption coefficient) and 0.744, respectively. In T2, the scattering coefficient is enlarged by 10% to 11 cm^{-1} , and the other coefficients are kept the same as in T1. In T3, only the absorption coefficient is enlarged by 10% to 11 cm^{-1} . In T4, the wavelength is modified to be 1800 nm in the simulation, and the g factor becomes 0.713 according

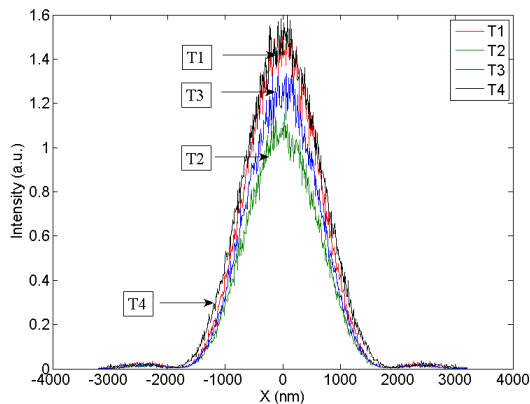


Figure 8. The simulated focal curves for simulation T1–T4, which are described in detail in Subsection 3.2.

to the Mie theory. The results for these four simulations are shown in Fig. 8, in which one sees that the focal intensity for T2 suffers the most severe deterioration. These results indicate that when the absorption and scattering coefficients are comparable, the scattering coefficient has greater impact on the focused spot. Therefore, Eq. (6) is no longer suitable to predict the penetration depth in LSM setup. Some EMC simulations are needed in order to derive the accurate penetration depth. The intensity curves for T1 and T4 are almost the same, apart from the small expansion of the T4 intensity curve for larger simulated wavelength. Hence, a small change in the g factor value (about 5%) hardly affects the focal intensity at a depth of 1.5 mm.

3.3. The Focal Beams Formed by Objectives with Different Numerical Apertures

When imaging the transparent biological sample, the objective with a higher NA gives rise to a stronger light intensity density in the focal

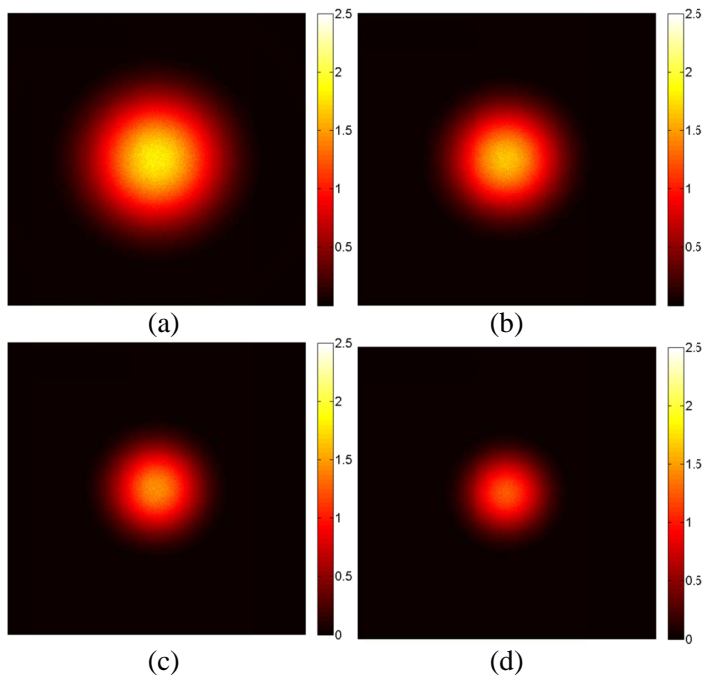


Figure 9. The focal spots within the biological sample through using objectives of different NA values. (a) NA = 0.4. (b) NA = 0.5. (c) NA = 0.6. (d) 0.7.

spot. However, as the NA of the objective gets larger, more of the light would impinge on the biological sample at a larger tilted angle. This part of light suffers more scattering than the part of normally incident light, and the coherence of the tilted incident light deteriorate more rapidly than that of the normally incident light [12]. EMC can also be utilized to ‘numerically’ study the focal spot formed by using objective lenses with different NA values. Herein, apart from the NA value of the objective, the other simulation parameters are the same as in simulation T1 described in Subsection 3.2. The simulated results are shown in Figs. 9 and 10. As the NA of the objective gets larger, the focal spot gets smaller. However, even with a smaller size, the intensity density of the focal spot obtained from a high NA objective is still less than that of the focal spot obtained from a low NA objective. The focal curves and intensity density for these four simulations are shown in Fig. 8 in detail. Therefore, the utilization of EMC simulation may also help people to choose a proper objective in tissue imaging.

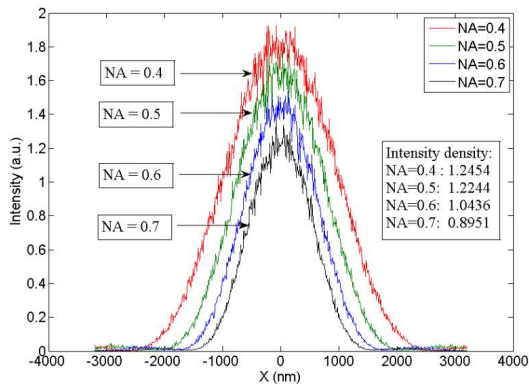


Figure 10. The intensity curves of focal spots through using objectives of different NA values.

4. CONCLUSION

In this study, the EMC simulation has been combined with the Huygens-Fresnel principle theory to derive the focal spot of laser beams. Through the hypothesis that the main absorption material in a biological sample between the 800 nm and 2400 nm range is water and the fact that the scattering coefficient can be calculated by the Mie theory, we can obtain the spectra for anisotropic factor, absorption coefficient and scattering coefficient of the biological sample. Using

these optical parameters, the intensity distribution of the focal laser beam with different wavelengths in deep tissue can be calculated. Based on our simulation results, 1680 nm is the best pump wavelength for microscopy in deep tissue. In addition, the 2220 nm pump laser is a proper optical source. Through the EMC method, we have further compared the effects of the anisotropic factor, absorption and scattering coefficients on the formation of focal laser spots. When the absorption and scattering coefficients are comparable, the scattering coefficient gives rise to the most deterioration on the focal spot, and the absorption coefficient follows. The change in the anisotropic factor hardly varies the intensity of the focal spot. Therefore, decreasing the scattering coefficient is critical for deep tissue imaging. Typically, the scattering coefficient has a smaller value in the long wavelength region. According to Abbe's theory, as the wavelength of the optical source gets longer while the NA of the objective keeps the same, the resolution of the microscopic image would be deteriorated. Another excellent method to extend the imaging depth is to use wavefront shaping [21], in which some shorter wavelength source can be utilized to explore deep tissue. This way both the imaging depth and resolution can be taken into account.

Finally, EMC simulations with objective lenses of different NA values have been performed to calculate the optical intensity density of the focal spot in the biological sample. Since the light focused by a higher NA objective would suffer more scattering events in EMC simulation, the optical intensity density decreased as the NA gets larger. However, the image obtained from a low NA objective may suffer a low signal to background ratio. Overall, more thorough optical properties of a biological sample at the focal spots can be studied by using EMC simulation. The present method also has the potential to help people optimize the optical parameters of the bio-imaging system.

ACKNOWLEDGMENT

This work was partially supported by the Science and Technology Department of Zhejiang Province (2010R50007), and the National Basic Research Program (973) of China (2011CB503700), the "111" Project, and SOARD.

REFERENCES

1. Boas, D. A., D. H. Brooks, E. L. Miller, C. A. Dimarzio, M. Kilmer, R. J. Gaudette, and Q. Zhang, "Imaging the body with

- diffuse optical tomography,” *IEEE Signal Process Mag.*, Vol. 18, No. 6, 57–75, 2001.
2. Karanasiou, I. S., N. K. Uzunoglu, and A. Garetos, “Electromagnetic analysis of a non-invasive 3D passive microwave imaging system,” *Progress In Electromagnetics Research*, Vol. 44, 287–308, 2004.
 3. Goharian, M., M. Soleimani, and G. R. Moran, “A trust region subproblem for 3D electrical impedance tomography inverse problem using experimental data,” *Progress In Electromagnetics Research*, Vol. 94, 19–32, 2009.
 4. Yodh, A. and B. Chance, “Spectroscopy and imaging with diffusing light,” *Phys. Today*, Vol. 48, 34–40, 1995.
 5. Kobat, D., M. E. Durst, N. Nishimura, A. W. Wong, C. B. Schaffer, and C. Xu, “Deep tissue multiphoton microscopy using longer wavelength excitation,” *Opt. Express*, Vol. 17, No. 16, 13354–13364, 2009.
 6. Horton, N. G., K. Wang, D. Kobat, C. G. Clark, F. W. Wise, C. B. Schaffer, and C. Xu, “In vivo three-photon microscopy of subcortical structures within an intact mouse brain,” *Nature Photonics*, Vol. 7, 205–209, 2013.
 7. Wang, P., H.-W. Wang, M. Sturek, and J.-X. Cheng, “Bond-selective imaging of deep tissue through the optical window between 1600 and 1850 nm,” *J. Biophotonics*, Vol. 5, No. 1, 25–32, 2012.
 8. Wang, L., S. L. Jacques, and L. Zheng, “MCML — Monte Carlo modeling of light transport in multi-layered tissues,” *Computer Methods and Programs in Biomedicine*, Vol. 47, No. 2, 141–146, 1995.
 9. Guo, Z., F. Cai, and S. He, “Optimization for brain activity monitoring with near infrared light in a four-layered model of the human head,” *Progress In Electromagnetics Research*, Vol. 140, 277–295, 2013.
 10. Pawley, J. B., *Handbook of Biological Confocal Microscopy*, Springer, New York, 2006.
 11. Xu, M., “Electric field Monte Carlo simulation of polarized light propagation in turbid media,” *Opt. Express*, Vol. 12, No. 26, 6530–6539, 2004.
 12. Hayakawa, C. K., V. Venugopalan, V. V. Krishnamachari, and E. O. Potma, “Amplitude and phase of tightly focused laser beams in turbid media,” *Phys. Rev. Lett.*, Vol. 103, 043903, 2009.
 13. Hayakawa, C. K., E. O. Potma, and V. Venugopalan, “Electric

- field Monte Carlo simulations of focal field distributions produced by tightly focused laser beams in tissues,” *Biomed. Opt. Express*, Vol. 2, No. 2, 278–299, 2011.
14. Wang, Y., P. Li, C. Jiang, J. Wang, and Q. Luo, “GPU accelerated electric field Monte Carlo simulation of light propagation in turbid media using a finite-size beam model,” *Opt. Express*, Vol. 20, No. 15, 16618–16630, 2012.
 15. Li, M., P. Lu, Z. Yu, L. Yan, Z. Chen, C. Yang, and X. Luo, “Vector Monte Carlo simulations on atmospheric scattering of polarization qubits,” *J. Opt. Soc. Am. A*, Vol. 30, 448–454, 2013.
 16. Hale, G. M. and M. R. Querry, “Optical constants of water in the 200-nm to 200- μ m wavelength region,” *Appl. Opt.*, Vol. 12, No. 3, 555–563, 1973.
 17. <http://refractiveindex.info/?group=LIQUIDS&material=Water>.
 18. Ding, H., J. Q. Lu, W. A. Wooden, P. J. Kragel, and X.-H. Hu, “Refractive indices of human skin tissues at eight wavelengths and estimated dispersion relations between 300 and 1600 nm,” *Phys. Med. Biol.*, Vol. 51, No. 6, 1479–1489, 2006.
 19. Xu, X. and W. W. Webb, “Measurement of two-photon excitation cross sections of molecular fluorophores with data from 690 to 1050 nm,” *JOSA B*, Vol. 13, No. 3, 481–491, 1996.
 20. Song, Y. J., M. L. Hu, C. L. Wang, Z. Tian, Q. R. Xing, L. Chai, and C. Y. Wang, “Environmentally stable, high pulse energy Yb-doped large-mode-area photonic crystal fiber laser operating in the soliton-like regime,” *IEEE Photonics Technology Letters*, Vol. 20, No. 13, 1088–1090, 2008.
 21. Wang, Y. M., B. Judkewitz, C. A. DiMarzio, and C. Yang, “Deep-tissue focal fluorescence imaging with digitally time-reversed ultrasound-encoded light,” *Nature Communications*, Vol. 3, 928, 2012.